Enhanced Catalytic Conversion of Benzaldehyde to Benzoic Acid using Silica Coated Hydrated Iron Oxide

U. A. Soliman, E. M. El-Telbani, H. A. Siddiq, M. M. El-Moselhy, S. R. Elgogary, M. S. Thabet, R. E. Azooz* and Z. H. Mohamed

Department of Physical Sciences, Chemistry Division, College of Science, Jazan University, Jazan, Saudi Arabia *Corresponding author: rramadan@jazanu.edu.sa

Received 19/05/2025; accepted 12/09/2025 https://doi.org/10.4152/pea.2027450403

Abstract

In this study, hydrated iron oxide-modified silicates (Si-Fe(n)) with varying iron concentrations were synthesized via one-step loading. Comprehensive characterization using N₂ adsorption-desorption, Fourier Transform Infrared spectrophotometer, Scanning Electron Microscope, Transmission Electron Microscopy, Energy-dispersive X-ray and X-ray Diffraction revealed that Fe incorporation preserved silica's phase composition and crystal structure (evidenced by consistent XRD peak broadening), achieved uniform iron distribution within silica matrix (EDX/TEM), with 12.5 nm average particle size, and enhanced surface area and Fe-bonded OH groups (FT-IR). These modifications correlated with improved catalytic performance in benzaldehyde oxidation, for which the reaction mechanism was elucidated.

Keywords; Benzaldehyde oxidation; catalysis; Density Functional Theory; Hydrated iron oxide modified silicates.

Introduction•

Carbonyl compounds are extensively used as intermediates in commercial and scientific settings, making oxidation an important step in organic synthesis. Several methods for converting aldehydes to carboxylic acids have been developed [1, 2]. Most often used oxidants include acidic permanganates and chromates, fuming nitric acid, aqueous sodium hydroxide-silver oxide, ozone and cyanide-silver oxide 2. Various oxidants have disadvantages, such as high cost, low selectivity, environmental effect and challenging working conditions [3].

Benzaldehyde is known to spontaneously undergo autoxidation, to form benzoic acid when exposed to air at ambient temperature (20 °C) [4]. The presence of catalysts like

-

[•] The abbreviations list is in pages 276-77.

transition-metal ions or free radical initiators such as benzoyl peroxide accelerates this oxidation [5]. Photochemical excitation also aids this transformation, and it is widely accepted that this reaction follows a radical chain process.

Catalysis is critical in modern manufacturing, as it reduces energy input, suppresses undesirable side reactions, and increases product output [6]. Catalysts lower the reaction energy barrier, accelerating chemical transformations without affecting reactants or products [7], being commonly employed in industrial synthesis since they are inexpensive, stable and easy to separate. Chemists and engineers have worked for decades to improve efficiency in a variety of procedures.

Hybrid Fe-silicate is a promising new type of porous material with unique compositions and structure frameworks, which have various applications, including water remediation, electrochemical energy storage, adsorption of As cations, catalysis and more [8-12].

Oxidation of aldehydes to acids, namely benzaldehyde to benzoic acid, is a significant transition process. Benzoic acid is a pertinent chemical and a precursor for manufacturing numerous other compounds, and is one of the most prevalent organic acids, being widely utilized in medicine, food processing and chemical industry. More than 90% of generic benzoic acid converts directly to phenol and caprolactam [13], which have widespread applications, including as rubber polymerization activators and in manufacturing of alkyd resins.

Oxidation of benzaldehyde to benzoic acid can be catalyzed by various compounds. Sodium tungstate dihydrate effectively catalyzes this reaction, with acidic additives and surfactants improving yield [14]. Ni/Al-hydrotalcite-like-compounds in acetic acid have stable activity and zero-order reaction kinetics [13]. Sulfonic acid resin catalyzes oxidation using hydrogen peroxide, with electron-withdrawing substituents enhancing reactivity [15]. Rhodium and palladium compounds also catalyze this reaction in a benzene solution under an oxygen atmosphere [16]. These diverse catalytic systems offer various approaches to efficiently oxidize benzaldehyde to benzoic acid under different reaction conditions.

This paper presents an environmentally friendly and cost-effective method for converting benzaldehyde to benzoic acid using a heterogeneous hybrid iron-modified silicate catalyst. Herein, the focus was on reaction kinetics and other characteristics that led to investigating a probable reaction mechanism. These fundamental discoveries may provide significant suggestions for further catalyst design and future research on oxidation of other aromatic aldehydes. The aim was to synthesize Si-Fe catalysts with controlled Fe loading, characterize their structural and surface properties, evaluate their catalytic performance in benzaldehyde oxidation, and elucidate the reaction mechanism through combined experimental and computational approaches.

Materials and methods

Synthesis of hybrid iron-modified silicate

To create iron-modified hybrid silicate, high-purity silica gel from Sigma Aldrich's (pore size 60 Å; mesh size 60-120), anhydrous NaOH pellets (reagent grade, ≥98%) and Fe₂(SO₄)₃ (anhydrous, powder, P 99.99% trace metals base) were used. 50 g silica gel were first treated with 1 M NaOH, kept under vigorous mechanical agitation for 10 min, and washed with ion-free water several times until neutralized. The neutralized material was divided into four equal portions and treated with certain amounts of a Fe₂(SO₄)₃ solution (prepared in deionized water (7 g Fe₂(SO₄)₃ per 100 mL solvent ~ 0.175 M). Each sample received a specific name to distinguish between different Fe-loadings.

Catalyst characterization

X-RD was recorded at room temperature using a Rigaku/Smart Lab diffractometer with non-monochromotographic Cu K α radiation (λ = 0.154 nm), operating at 40 kV and 100 mA. Measurements were taken at scanning speed of 8° (20)/min at a scanning range from 5 to 65°.

SEM (JEOL/JSM-6610) and EDX (Oxford Instruments Inca X-Act/51-ADD0013) were used to examine surface morphology and particle size of iron-loaded samples, for creating a comprehensive map of resulting hybrid iron-modified silicates. In addition, a JEOL-2100 TEM was employed to evaluate produced samples.

The specific surface area of samples and micropore volume were determined by collecting N_2 adsorption-desorption utilizing Autosorb 1C for surface area and ASAP2020 for pore size distribution, at - 196 °C. Samples were evacuated, heated to 200 °C, again evacuated until a pressure of 1.3 Pa was achieved, and maintained overnight before adsorption. Multipoint BET, t-plot and DR were used to determine surface area, total pore volume and micropore volume, respectively.

Specific surface area and pore diameter of synthesized samples were measured on an automatic Micrometrics ASAP2020 instrument (made in the USA) by nitrogen adsorption. Before testing, the instrument was set to a temperature of 100 °C, for silica and 200 °C for Si-Fe, to ensure complete moisture removal without structural damage, and a pressure of 101.325 kPa, for 5h in advance. The adsorbate was high-purity nitrogen. Surface areas were determined by BET method from nitrogen adsorption data. Pore diameter and size distribution were determined by BJH method. Morphologies and dimensions of synthesized products were examined using a JEOL JSM-6700F field emission-SEM.

Atomic absorption spectroscopy (AAS) (GB CA 4382) was used to measure the amount of iron loaded in supernatants. Before AAS analysis, 0.1 g of all samples were treated with 10 mL (2 M) HCl, to leach out precipitated iron hydroxide, which allowed estimate iron content of silica.

Infrared adsorption measurements were carried out using a FT-IR spectrophotometer (Bruker Optics-Alpha) for Si and iron-loaded Si samples. FT-IR spectra were collected in 400≈4000 cm-1 wavenumber region, with a resolution of 4 cm−1, using a single bounce ATR with diamond crystal.

Oxidation of benzaldehyde to benzoic acid

A 250 mL three-necked flask, with a fixed condenser and thermometer, was fixed to a DF-101S magnetic force stirrer. 25 mL benzaldehyde were added with or without 50 mg catalyst (Si-Fe or Si-blank pretreated as described earlier). Water cooling was used to reflux and stir at the required temperature for a predetermined amount of time (8 h). The reaction mixture, obtained considering time, catalyst dose and required temperature, was refluxed and monitored using thin-layer chromatography. After the reaction was completed, the mixture was cooled, filtered, dried and crystallized from hot water, to yield benzoic acid as white crystals, with 96% yield (Rf = 0.39, pet. ether: ethyl acetate, 10:1), m. p. 121-122 °C. The obtained product (benzoic acid) was confirmed by measuring its melting point and infrared spectra.

Results and discussions

Sample characterizations

Powder X-RD analysis

Fig. 1 shows X-RD patterns of silica gel and hybrid iron-modified silicate samples with varying Fe contents.

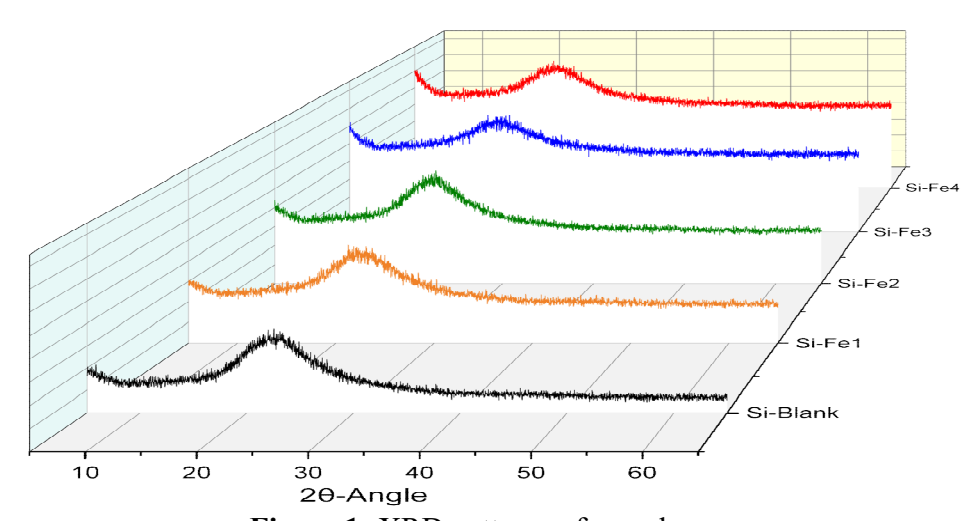


Figure 1: XRD patterns of samples.

All samples had an amorphous form, without any diffraction lines indicating the presence of Fe-O species [8, 17, 18]. The differences in peak positions and intensities show that Fe doping did not change either crystalline structure or phase composition

of Si samples. This finding could reflect that iron well dispersed inside the silicate matrix, still retaining the same crystallographic nature even after the modification process. Furthermore, the absence of diffraction lines that could be assigned to the presence of HFO phase might indicate that incorporated HFO species occupy interstitial positions inside the silicate matrix and/or on the silicates surface with a very small particle size below detection limit of the instrument.

SEM and EDX spectroscopy

The two components in Fig. 2 are an SEM spectrum, on the right, and an EDX layered image on the left.

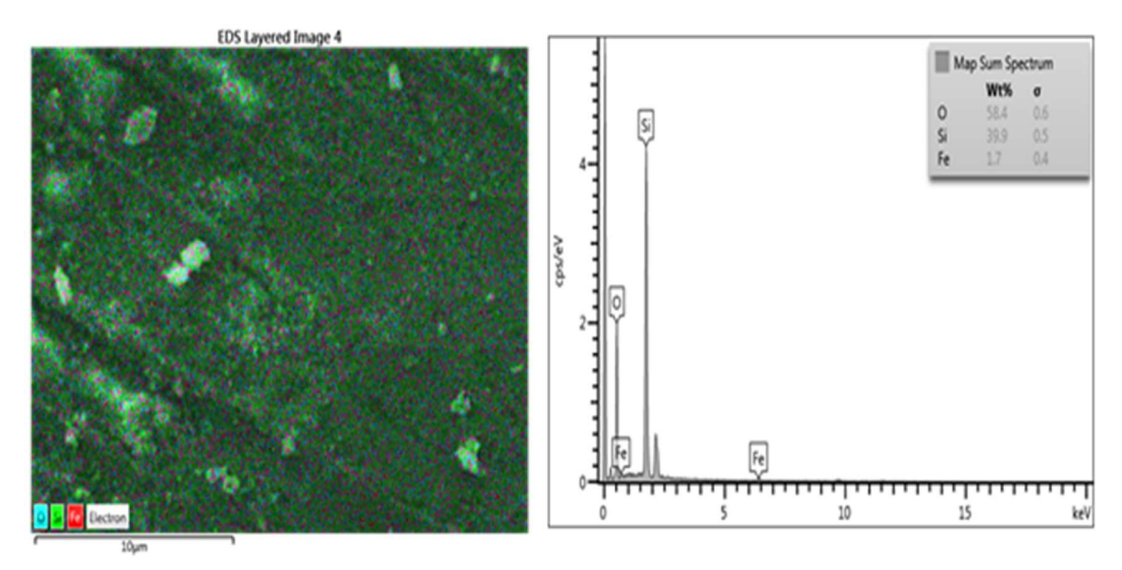


Figure 2: SEM image and EDX mapping of Si-Fe4.

EDX layered image shows a microscopic view of a sample with different elements highlighted in different colors. The green color indicates a high content of oxygen throughout the sample, showing that it is a major component of the matrix; the blue color indicates a significant presence of silicon, which likely forms the core structure of the sample side by side with oxygen; and the red color indicates a well distributed iron species on the surface, which is mainly localized along the examined specific areas. A homogeneous matrix is suggested by the distribution of different silica gel and HFO species, reflecting the success of the modification process, and keeping the main structure of silicate matrix intact, even after HFO incorporation.

On the other hand, EDX spectrum interpretation for iron peak (0.7 keV) reveals that is it a minor component, while the one from oxygen was 0.5 keV. Silicon's peak at 1.8 keV is prominent, confirming it is the major constituent. A quantitative assessment of the components is also given by weight percentages (Wt%) and standard deviations

(σ). Low standard deviations and a high percentage of silicon and oxygen suggest consistent and trustworthy data. The somewhat higher standard deviation and low percentage of iron point to distributional variability.

According to statistics, only a small portion of loaded iron is visible on the surface, since most of it is hidden. EDX suggests Fe incorporation within the silica matrix rather than surface deposition, since the iron burden was evenly distributed throughout the silica matrix.

Fig. 3 shows a TEM image of a Si-Fe4 sample.

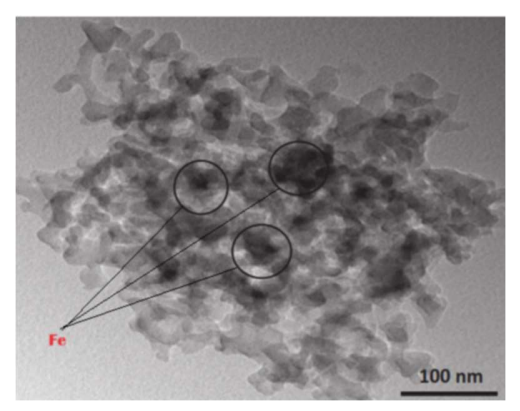


Figure 3: Tunneling TEM image of Si-Fe4.

The sample appears to be composed of a network of interconnected particles or clusters. The multi-distributed dark spots that are circled and marked with "Fe" in red indicate that iron is uniformly distributed inside the silicate matrix and that it exists with lower density on the surface, which might support the result obtained from XRD. Localized iron plays a specific role in the functionality of the material. For example, iron can act as a catalytic site or as an activator to modify the electronic properties of the material [19]. The distribution of iron can also affect the magnetic properties of the material [20], which may be relevant for certain applications. The image reveals a complex network of interconnected particles, indicating a high degree of porosity and surface area. This structure is typical of materials designed for applications such as catalysis, energy storage or adsorption. The particles appear to be relatively uniform in size, with diameters in the tens of nanometers range ($\leq 12.5 \ nm$). The morphology of the particles is irregular, which can influence the properties of the materials, such as their catalytic activity or adsorption capacity. Loaded iron is mostly found inside the silicate matrix with nano average sizes, which is outside the range of XRD detection.

Surface area measurements

Adsorption isotherms of the various materials are shown in Fig. 4 Si-Blank exhibits moderate adsorption capacity, with the adsorbed volume at $P/P_0 = 1.00$ reaching

around 200 cm³/g⁻¹. In contrast, Si-Fe¹ exhibits a higher adsorption capacity, with the adsorbed volume at $P/P_0 = 1.00$ reaching about 300 cm³ g⁻¹. Si-Fe² has a marginally greater adsorption capacity than Si-Fe¹, reaching about 320 cm³/g⁻¹ at $P/P_0 = 1.00$, with an adsorbed volume of around 380 cm³/g⁻¹ at $P/P_0 = 1.00$. Si-Fe₃ shows the highest adsorption capacity of all samples. Si-Fe⁴ has a lower adsorption capacity than Si-Fe₃, but greater than that from Si-Blank, with an adsorbed volume of about 250 cm³/g⁻¹ at $P/P_0 = 1.00$.

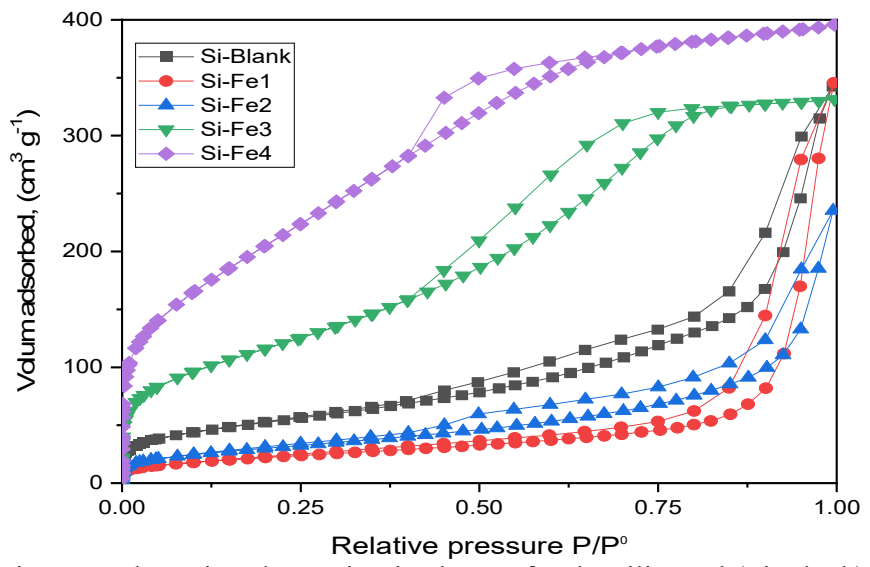


Figure 4: Nitrogen adsorption-desorption isotherms for the silica gel (Si-Blank) and hybrid iron-modified silicate (Si-Fe1 to Si-Fe4) samples.

Type II isotherms with characteristic upward deviation hysteresis loops are shown by Si-Blank, Si-Fe₁ and Si-Fe₂, which may support the porous nature of the surface both before and after iron modification. The central portion of the flatter zone lies between P/Po = 0.1-0.4 and 0.1-0.6, respectively, indicating the formation of a monolayer. Furthermore, the monolayer formation was initiated at the first point of monolayer saturation through micropores filled with nitrogen gas at very low pressures. Conversely, capillary condensation happened at higher pressure levels, while multilayer development occurred at middle-pressure levels.

Type IV isotherm, with shorter upward deviation hysteresis loops, as seen in Si-Fe₃ and Si-Fe₄ samples, indicates mesoporous materials with capillary condensation occurring at higher relative pressures. Hysteresis loops observed in isothermal curves suggest presence of mesoporous materials and occurrence of capillary condensation and evaporation.

Additionally, as shown in Table 1, the sharp rise in the isotherm at the point of monolayer saturation at low pressure indicates a high surface area. BET surface area

indicates that silica gel has a surface area of 190.3 m²g⁻¹. Upon loading, the surface area of the hybrid iron-modified silicate decreases to 82.2 and 110.8 m²g⁻¹, for Si-Fe₁ and Si-Fe₂, respectively. Furthermore, as Table 1 shows, increasing the iron loading to three or four times (Si-Fe₃ and Si-Fe₄) results in extremely large surface areas (426.9 and 781.7 m²g⁻¹, respectively). Resultant large surface areas may be due to relative dispersion of iron to occupy interstitial matrix spaces in silica matrix. Pore volume calculations show that samples treated with silica gel and iron have distinct pore sizes based on how much hybrid iron-modified silicate is loaded. In addition, according to the findings, Si-Fe₄ shows marginally higher pore volume (0.62 vs. 0.53 cm³/g) compared to Si-Fe₂, making it highly suitable for adsorption applications. Additionally, micropore volume evaluations show that microporosity decreases with increasing iron content.

TC 1.1 1 C1	•	C	1	1		C '1'	• •	1 1.
Table 1: Change	S 111	surface ar	eas and	nore chara	cteristics (าโ รปปกล	concerning iron	เกลสเทช
Table 1. Change	5 111	surrace ar	cus ana	pore chara		or office	concerning non	rouding.

Sample	Multipoint BET method	Volume adsorbed at p/p0 = 0.99	Micropore volume calculated by DR	DP
	SBET (m ² g ⁻¹)	V _{total} (cm ³ /g ⁻¹)	$ m V_{micro}$ (cm^3/g^{-1})	(A)
Si-Blank	190.3	0.53	0.077	55.8
Si-Fe1	82.2	0.54	0.03	130.9
Si-Fe2	110.8	0.37	0.008	65.1
Si-Fe3	426.9	0.53	0.029	24.2
Si-Fe4	781.7	0.62	0.022	15.6

Fourier transform infrared spectroscopy (FT-IR)

The most prominent band in FT-IR spectrum (Fig. 5) of parent silica gel appears at around 1100 cm⁻¹, which corresponds to asymmetric stretching vibration of Si-O-Si bonds [21, 22].

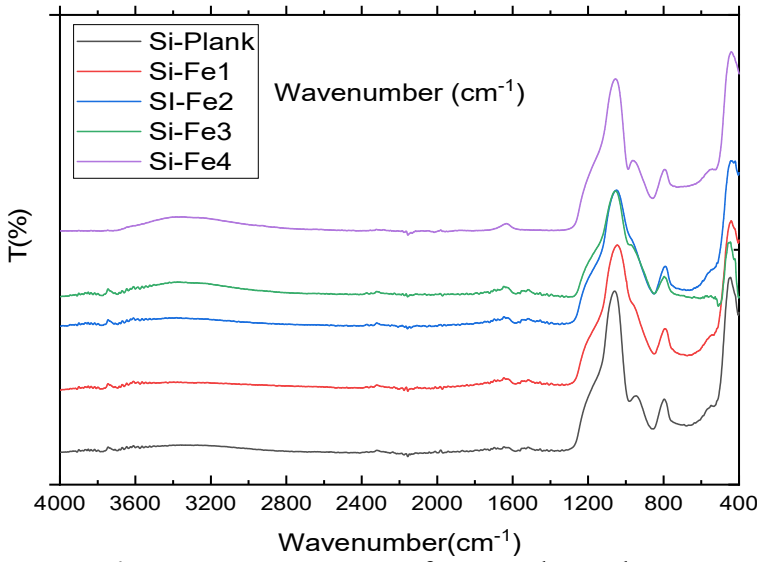


Figure 5: FT-IR spectra of prepared samples.

The broad band around 3400-3700 cm⁻¹ is attributed to stretching vibrations of surface silanol groups (Si-OH), and their intensities increase with higher amounts of Fe loaded, which may be due to the increasing surface area and OH groups attached to Fe sites. Bands around 800 and 460 cm⁻¹ are assigned to symmetric stretching and bending vibrations of Si-O-Si bonds, respectively [21- 24]. The peak at 1621 cm⁻¹ is due to O-H bending mode of water molecules.

Oxidation of Benzaldehyde to Benzoic acid

Effect of duration time

In the absence of a catalyst sample (Si-Fe4), benzaldehyde was not converted to benzoic acid under all reaction conditions. When 0.1 g Si-Fe4 was introduced into the reaction mixtures (as previously mentioned), the mixture was cooled overnight before being filtered, washed and dried, to provide a white crystal product. The product was weighed, and the isolated yield was determined using benzaldehyde contained in the reaction flask. The melting point of the product was 121-122 °C which is too close to results of [25] and [26]. IR (KBr) spectrum of white yield shows strong O-H stretching at 2500-3300 cm⁻¹, strong C=O stretching at 1680-1750 cm⁻¹, medium C-O stretching at 1300 cm⁻¹ and medium C-H bending of benzene ring at 900-1100 cm⁻¹. These results confirm the formation of benzoic acid due to oxidation of benzaldehyde in presence of a Si-Fe₄ catalyst. Other catalysts are used and obtained data are shown in Fig. 6.

$$Si - Blank < Si - Fe_1 < Si - Fe_2 < Si - Fe_3 < Si - Fe_4$$

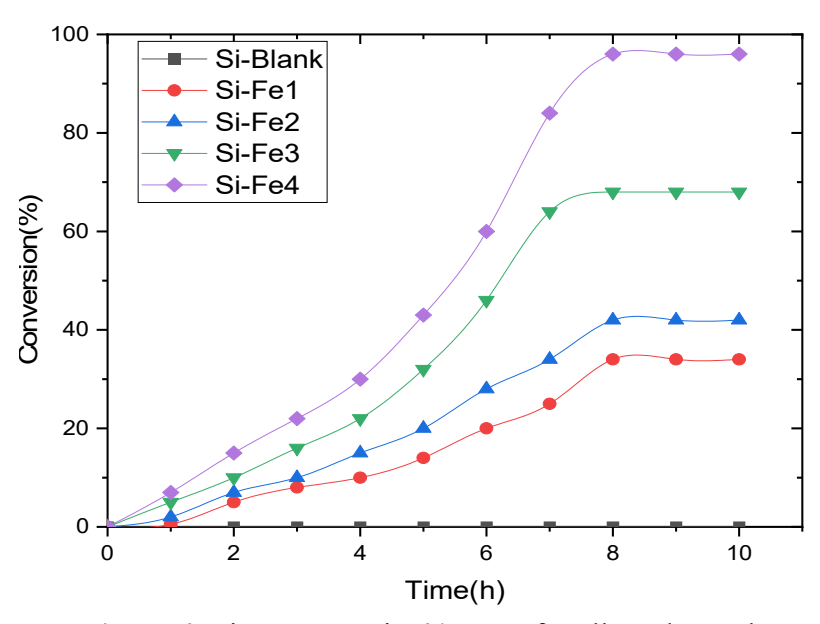


Figure 6: Time-conversion% curve for all used samples.

The graph shows that iron-modified silicates (Si-Fe₁ to Si-Fe₄) are more efficient catalysts for conversion of benzaldehyde to benzoic acid than unmodified silicate (Si-Blank). All iron-modified catalysts show an increase in conversion percentage over time, but conversion rate varies significantly among them. Among iron-modified catalysts, Si-Fe₄ shows highest catalytic activity, achieving nearly 100% conversion within 8 h. This indicates that the amount and distribution of iron play a crucial role in enhancing catalytic performance. Catalyst efficiency reaches ~96% for Si-Fe₄ and the order increases as follows:

Other catalysts used in the oxidation of similar compounds are illustrated in Table 2.

Catalyst/medium	Outcome measured	yield%	Ref.
$Na_2WO_4 \cdot 2H_2O - H_2O_2$	Benzaldehyde to benzoic acid	70-90%	[14]
NiAl-hydrotalcite-like-	Benzaldehyde to benzoic acid		[13]
transition metal complexes	Oxidation of benzaldehyde to benzoic acid and perbenzoic acid	Up to 83%	[16]
V_2O_5 , SnO ₂ -promoted V_2O_5 , and	Oxidation of benzaldehyde to benzoic acid	Up to 53%	[27]
Copper-based binary metal oxide	Toluene to benzaldehyde, and with a longer reaction time, to	Up to 25%	[28]
Co/ZSM-5	Styrene to benzaldehyde and benzoic acid	100%	[29]
Copper-iron-polyphthalocyanine	Oxidation of benzaldehyde to benzoic acid.	Up to 55%	[30]
Nickel(II) complex /O ₂ /different	Oxidation of aldehydes into carboxylic acids	Up to 91%	[31]
Methyltrioxorhenium /H ₂ O ₂ /	Oxidation of benzaldehydes to phenols	75% for phenol	[32]
MoO_2/H_2O_2	Oxidation of benzyl alcohol to benzaldehyde.	94%	[33]
Water-soluble palladium(II)	Green, catalytic oxidation of a wider range of alcohols.	93%	[34]
Ir(III) Rh(III) and Pd(II) with	Oxidation of benzaldehyde to benzoic acid	82%	[35]

Table 2: Some catalysts used in the oxidation of organic compounds.

Effect of catalyst doses

Si-Fe₄ was herein used as the best catalysis sample, to change the dose and track conversion at 80 °C. Resulting data is shown in Fig. 7A, where an increase in additional dose improves conversion rate.

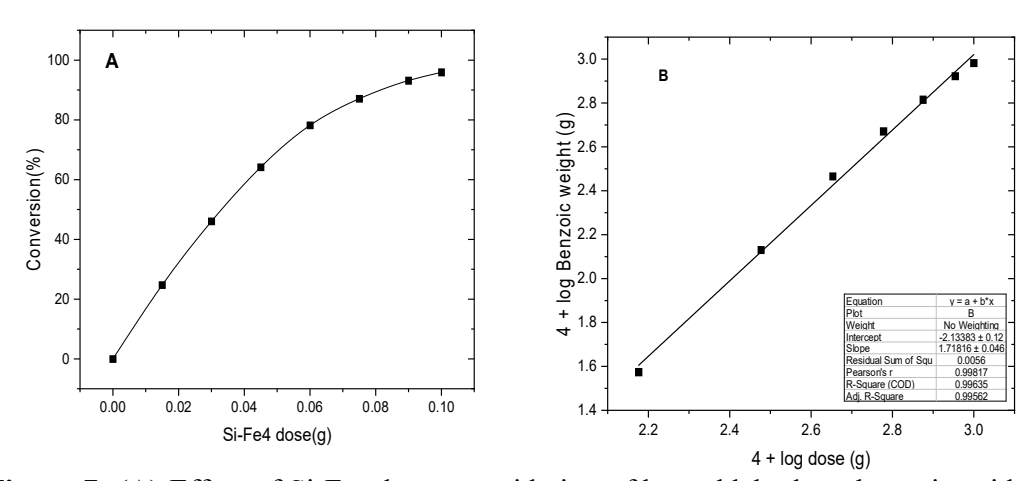


Figure 7: (A) Effect of Si-Fe₄ dose on oxidation of benzaldehyde to benzoic acid at 80 °C; **(B)** Double logarithmic plot of the benzoic yield versus Si-Fe₄ doses.

In Fig. 7B, a straight line ($r^2 = 0.998$) with a slope of 1.72 illustrates linear behavior. Si-Fe₄ dose-related reaction order is therefore second-order.

Effect of temperature

At 8 h and Si-Fe₄ dose of 0.1 g, conversion ratio was studied by changing the reaction temperature. Obtained data are plotted in Fig. 8A, which shows a positive correlation between temperature and conversion ratio, indicating that, with higher temperatures, conversion percentage increases.

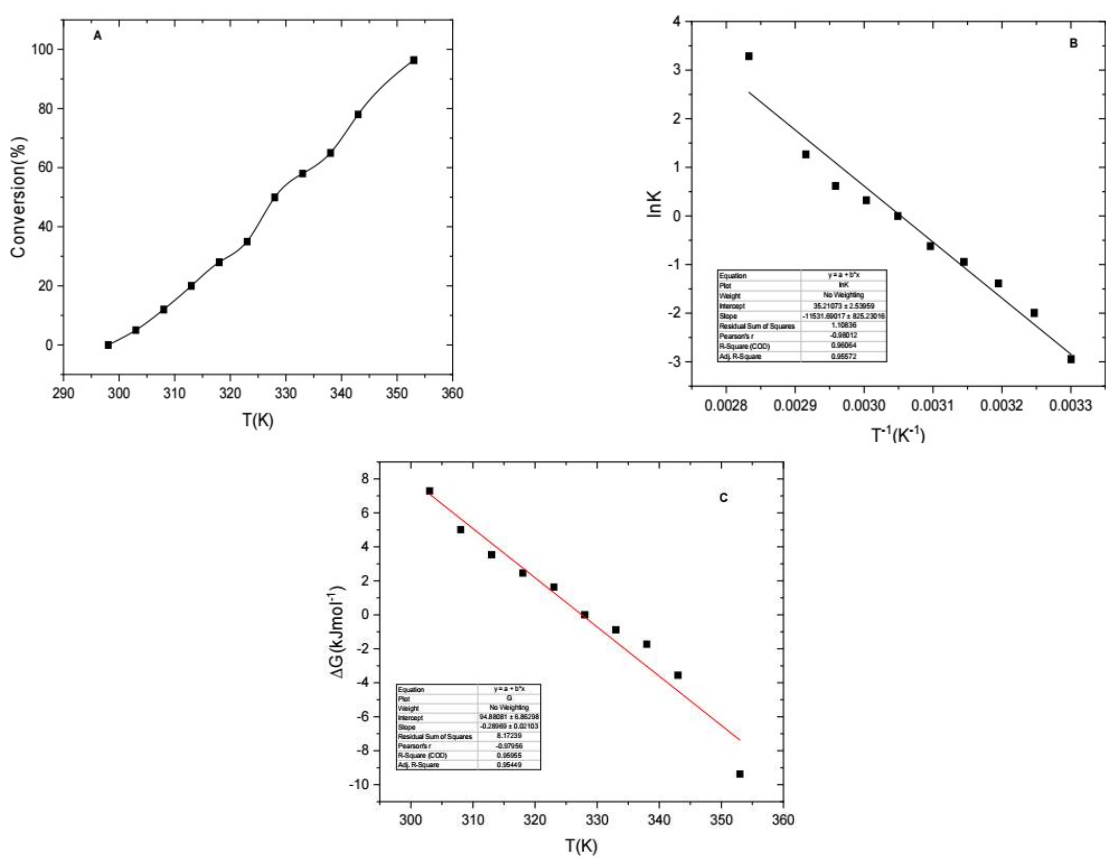


Figure 8: (A) Effect of temperature on oxidation of benzaldehyde, (B) Arrhenius plot relationship and (C) Free energy -temperature relationship.

Computational study

DMol³ calculation model, part of Materials Studio v2023, was used to optimize the geometry of this molecule. Electronic properties were functional GGA/PBE, zero charge and controlled spin polarization. Each electron in core treatment is regarded as part of DNP Basis set. Table 3 lists calculations for E_{HOMO} and E_{LUMO} are visually shown in Fig. 9. E_{HOMO} and E_{LUMO} are used to determine energy gap (ΔE), global

hardness (η), global softness (S), ionization potential (I), electron affinity (A), absolute electronegativity (x) and global electrophilicity index (ω).

Compound	Fe(OH) ₃	Benzaldehyde	Benzoic acid
ЕНОМО	-5.769	-5.544	-6.099
ELUMO	-4.835	-2.572	-2.302
$\Delta E_{(HOMO-LUMO)}$	-0.934	-2.972	-3.797
Ionization energy (I)	5.769	5.544	6.100
Electron affinity (A)	4.835	2.572	2.303
Electronegativity (X)	5.302	4.058	4.201
Global hardness (η)	0.467	1.486	1.898
Chemical potential (π)	-5.302	-4.058	-4.201
Global softness (σ)	2.142	0.673	0.527
Global electrophilicity (ω)	30.109	5.542	4.648
Electron accepting $(\omega +)$ power	27.516	3.698	2.785
Electron donating (ω-) power	32.819	7.7578	6.985
Net electrophilicity ($\Delta \omega$ +-)	60.335	11.455	9.770

Table 3: Calculated quantum chemical parameters.

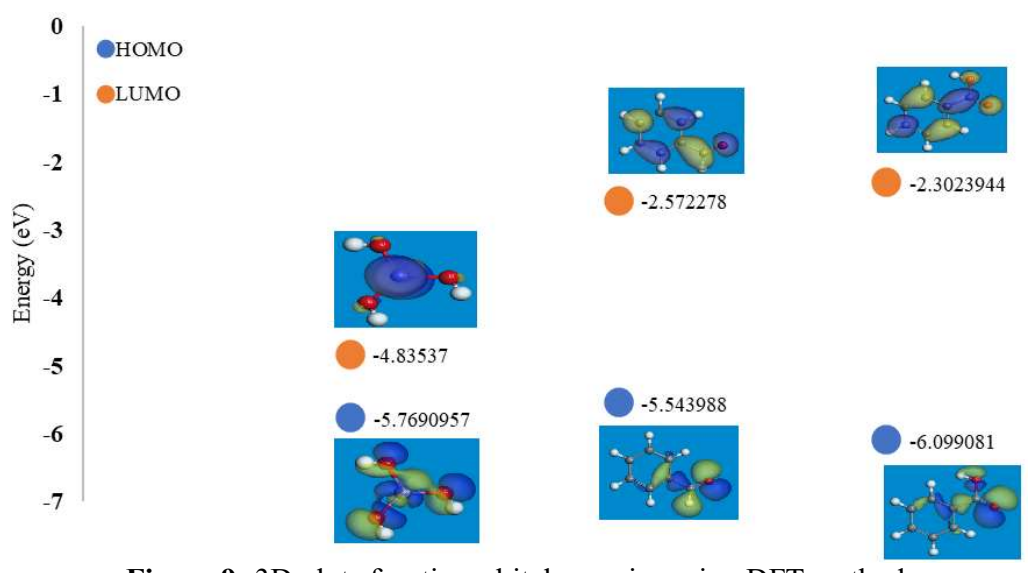


Figure 9: 3D plots frontier orbital energies using DFT method.

Table 3 depicted that energy gap between E_{HOMO} and E_{LUMO} was the lowest for $Fe(OH)_3$ (-0.934 eV), indicating it has the highest reactivity and lowest stability. In contrast, Benzoic acid has the largest energy gap (-3.797 eV), suggesting it is the most stable and least reactive. $Fe(OH)_3$ shows highest electrophilicity, lowest stability and maximum reactivity. It is extremely reactive because it is a powerful electron donor and acceptor. Moderate stability and reactivity are displayed by benzaldehyde, which is more electrophilic than benzoic acid but less than $Fe(OH)_3$. The most stable and least reactive substance is benzoic acid. Out of the three compounds, it is the hardest and least electrophilic.

The interaction between Fe(OH)₃, benzaldehyde and benzoic acid was investigated using adsorption-desorption module. The resulting three-dimensional structure is shown in Fig. 10, where it can be seen that the bond in benzaldehyde/Fe(OH)₃ system is shorter. This confirms strong adsorption and possible coordination bond formation, while longer bonds in Fe(OH)₃/benzoic acid indicate that it can be more easily removed from the catalyst compounds' surfaces. Calculated binding energy is also stronger for benzoic acid/Fe(OH)₃ (2.483 kcal/mol⁻¹) compared with benzaldehyde/Fe(OH)₃ (2.347 kcal/mol⁻¹), as shown in Fig. 10. Adsorption parameter is tabulated in Table 4, where a negative value indicates that adsorption process is exothermic, which means that energy is released when the compound adsorbs onto Fe(OH)₃. After benzaldehyde molecules are adsorbed onto the catalytic surface, accumulation occurs, and coordination bonds may form between them. Then, adsorbed benzaldehyde (E_{adsorption} = -5.516 kcal/mol⁻¹) was oxidized to form benzoic acid, which was still strongly adsorbed onto the catalyst surface, as it will be discussed about this mechanism.

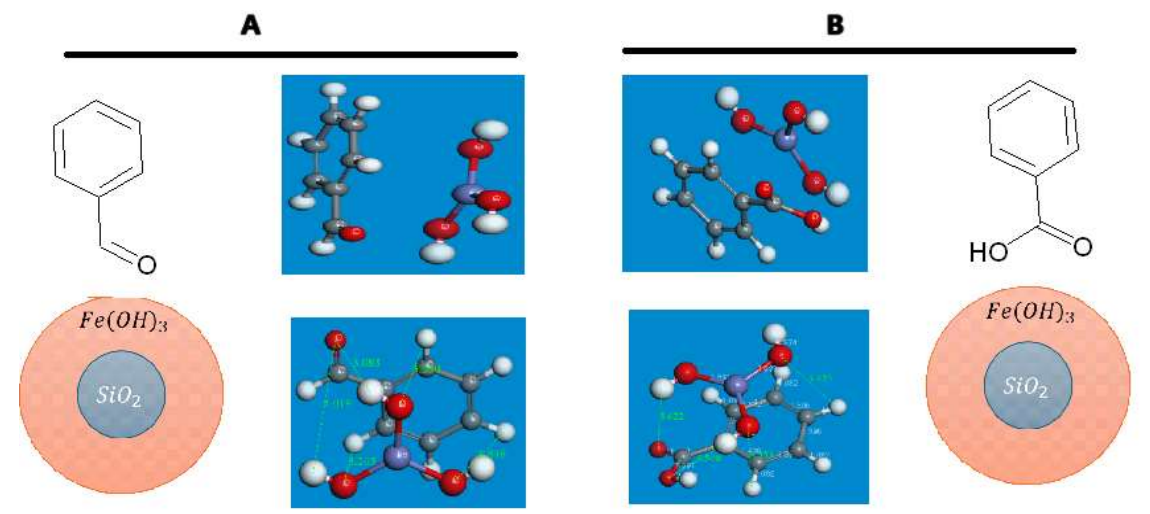


Figure 10: 3D plots frontier orbital after adsorption using DFT method- **(A)** Fe(OH)₃/benzaldehyde; **(B)** Fe(OH)₃/Benzoic acid.

Table 4: Adsorption parameter by MD (Monte Carlo simulation) Material studios.

Structures	Total energy (kcal/mol ⁻¹)	Adsorption energy (kcal/mol ⁻¹)	Rigid adsorption energy (kcal/mol ⁻¹)	Deformation energy (kcal/mol ⁻¹)	dE _{ad} /dN _i (kcal/mol ⁻¹)
Fe(OH) ₃	0000				
Benzoic acid	30.477				
Benzaldehyde	15.356				
Fe(OH) ₃ /Benzaldehyde	9.840	-5.516	-2.760	-2.756	-5.516
Fe(OH) ₃ /Benzoic acid	14.269	-16.209	-2.840	-13.369	-16.209

Total density of states (TDOS) and projected density of states (PDOS) were calculated to investigate electronic properties of silica gel loaded with Fe(OH)₃, benzaldehyde and benzoic acid, as well as their adsorbed complexes (Figs. 11 and 12). For Fe(OH)₃ (Fig. 11A), TDOS exhibits a continuous spread from valence to conduction band, with a prominent peak at -1.99 eV (7.56 7.56 DOS/eV), indicating strong electronic activity near Fermi level—a feature beneficial for electrochemical applications [36].

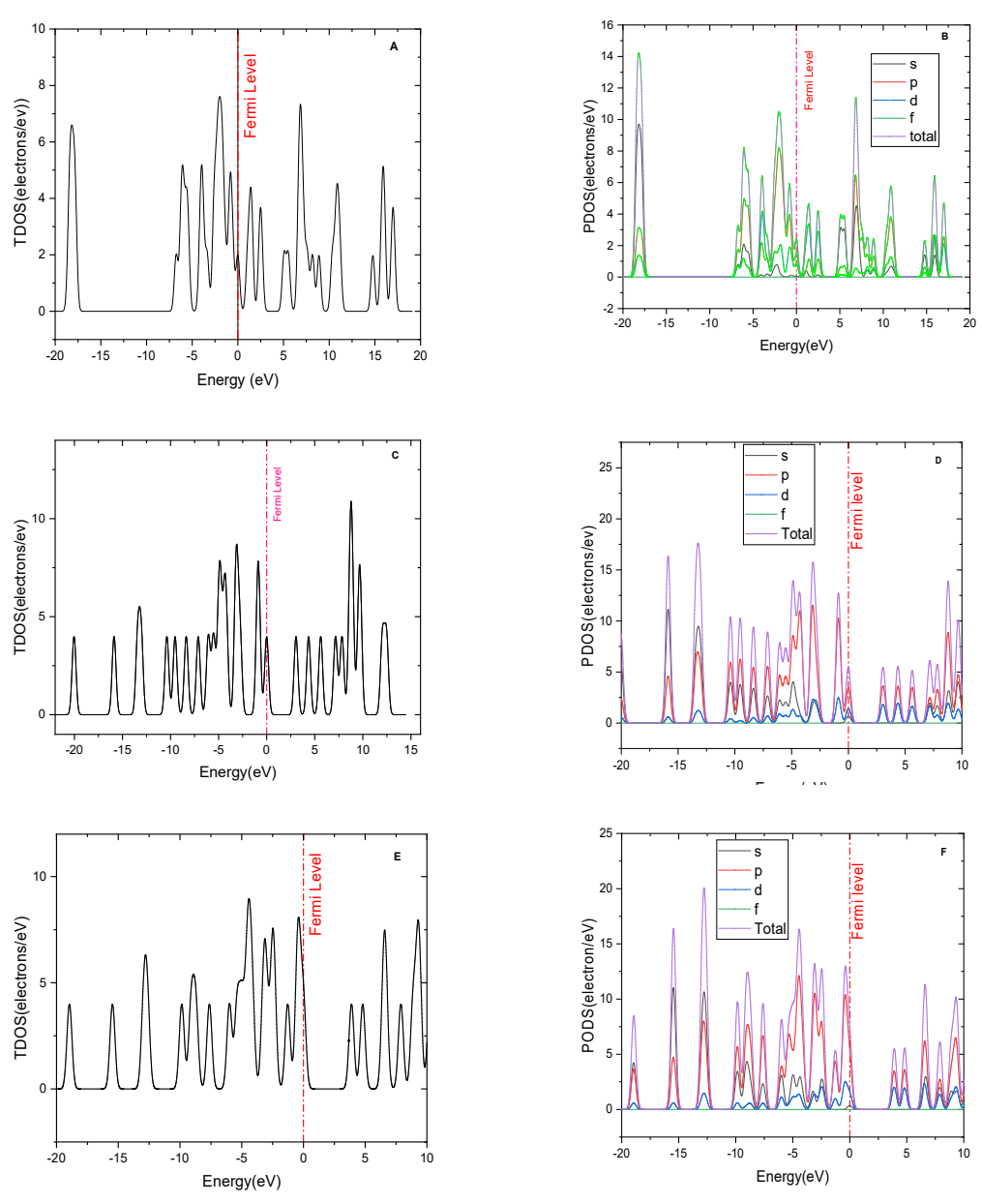


Figure 11: TDOS of **(A)** Fe(OH)₃; **(C)** benzaldehyde; **(E)** benzoic acid - and PDOS of; **(B)** Fe(OH)₃; **(D)** benzaldehyde; **(F)** benzoic acid.

PDOS (Fig. 11B) reveals dominant contributions from Fe ([Ar]3d⁶4s²) and O ([He]2s²2p⁴), particularly through their d, p and s orbitals, which hybridize strongly near Fermi level. In benzaldehyde (Fig. 11C) and benzoic acid (Fig. 11E), multiple TDOS peaks suggest conductive electronic states, while their PDOS plots (Figs. 11D and 11F) highlight significant p and d orbital contributions (–10 to –5 eV), with minimal involvement from f and s orbitals.

Further analysis of adsorbed systems (Fig. 12) reveals key bonding mechanisms. TDOS of Fe(OH)₃/benzaldehyde (Fig. 12A) and Fe(OH)₃/benzoic acid (Fig. 12B), along with their PDOS (Figs. 12C and 12D), demonstrate strong p-d hybridization (–10 to –5 eV), implying interactions between p orbitals of organics and d orbitals of Fe(OH)₃. This suggests coordination bonding between carbonyl groups (benzaldehyde/benzoic acid) and Fe(OH)₃'s oxygen atoms. High density of states near Fermi level in these systems underscores their electronic stability and robust bonding interactions, critical for catalytic behavior.

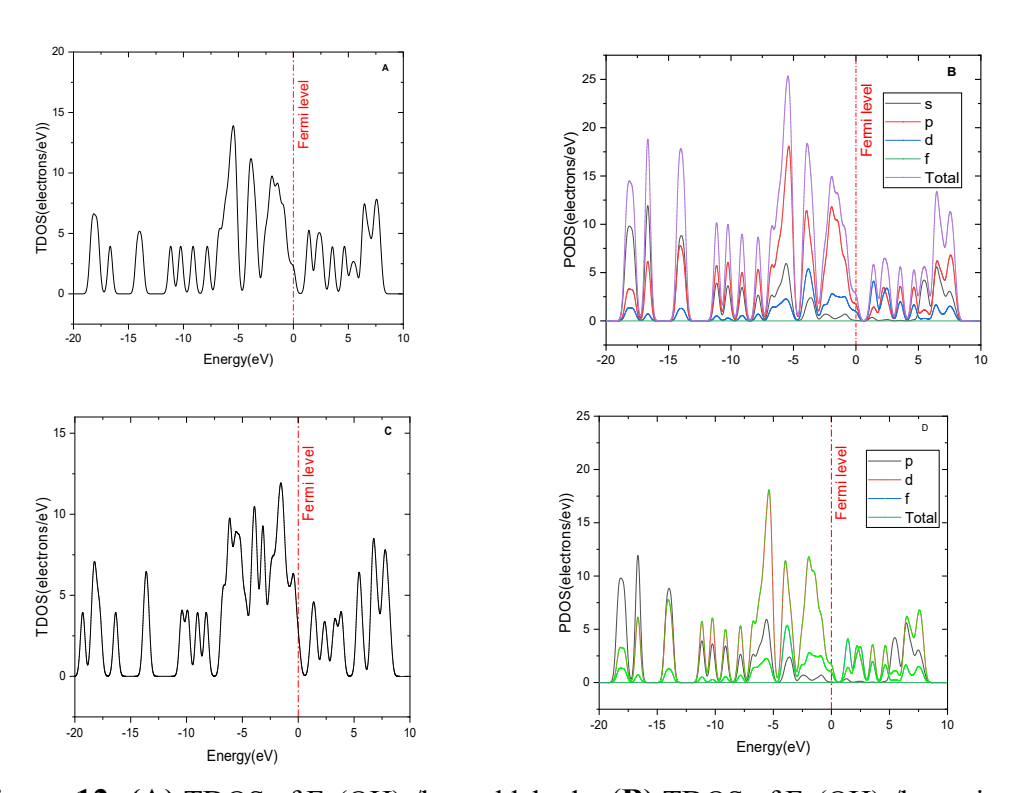


Figure 12: (A) TDOS of Fe(OH)₃/benzaldehyde; (B) TDOS of Fe(OH)₃/benzoic acid; (C) PDOS of Fe(OH)₃/benzaldehyde; and (D) PDOS of Fe(OH)₃/benzoic acid.

Reaction mechanism

SiO₂ modified with Fe(OH)₃ acts as heterogeneous catalyst for oxidation of benzaldehyde to benzoic acid. Fe(OH)₃ catalyst has active sites for oxidation reaction,

and SiO₂ support improves its dispersion, increasing the surface area and stability. Benzaldehyde (C₆H₅CHO) adsorbed onto the of the Fe(OH)₃/SiO₂ catalyst surface (eq. 1) as described by PDOS analysis. Molecular oxygen (O₂) in the air activates Fe(OH)₃ sites, generating reactive oxygen species as hydroxyl radicals (•OH) (eq. 2). Adsorbed benzaldehyde is oxidized to benzoic acid (C₆H₅COOH) by activated oxygen species, as shown in Eq. (3). Overall reaction is described in Eq. (4).

$$C_6H_5CHO$$
 (benzaldehyde) + $Fe(OH)_3/SiO_2 \rightarrow C_6H_5CHO - Fe(OH)_3/SiO_2$ (1)

$$O_2 + Fe(OH)_3 \rightarrow Fe(OH)_3 - O_2 \rightarrow Fe(OH)_3 - \bullet OH$$
 (2)

$$C^{6}H^{5}CHO - \frac{Fe(OH)^{3}}{SiO^{2}} + Fe(OH)^{3} - \bullet OH \rightarrow C^{6}H^{5}COOH \text{ (benzoic acid)} + Fe(OH)_{3}/SiO_{2} OH$$
 (3)

$$C_6H_5CHO + O_2 \rightarrow Fe(OH)_3/SiO_2C_6H_5COOH \tag{4}$$

Conclusions

SiO² increases the surface area of the catalyst, while temperature and iron content regulate conversion yield. Higher temperatures improve conversion rate, lower activation energy and improve thermodynamics of the reaction. Si-Fe system offers higher activity than unmodified silica or homogeneous Fe catalysts under mild conditions. Si-Fe4 is a superior catalyst for benzaldehyde oxidation to benzoic acid, with a conversion approach 96% at 08 °C. Computational calculation confirmed high reactivity of Fe(OH)₃, and its high tendency to accept electrons. TDOS and PDOS for Fe(OH)₃, benzaldehyde and benzoic acid showed similar overall shapes, but differed in peak intensities and positions. This indicates variations in electronic structure, due to different chemical environments. Further studies on catalyst reusability and substrate scope are warranted.

Authors' contributions

U. A. Soliman: conceptualization; methodology. E. M. El-Telbani: data curation; formal analysis. H. A. Siddiq: investigation; validation. M. M. El Moselhy: resources; visualization. S. R. Elgogary: writing – original draft. M. S. Thabet: supervision; project administration. R. E. Azooz: writing – review and editing; supervision. Z. H. Mohamed: writing; formal analysis.

Abbreviations

BET: Brunauer, Emmett and Teller **BJH**: Barrett, Joyner and Halenda

DR: Dubinin-Radushkevic **EDX**: energy-dispersive X-ray

FT-IR: Fourier Transform Infrared spectrophotometer

HFO: hydrated iron oxide

PDOS: projected density of states

SEM: scanning electron microscope

TDOS: Total density of states

TEM: transmission electron microscopy

XRD: X-ray diffraction

References

- 1. Smith M. Organic Synthesis; Academic Press, 2016.
- 2. Le Paih J, Frison J-C, Bolm C. Oxidation of Carbonyl Compounds. Modern Oxidation Methods. 2004: 253-265.
- 3. Guo Z, Liu B, Zhang Q et al. Recent advances in heterogeneous selective oxidation catalysis for sustainable chemistry. Chem Soc Rev. 2014;43(10):3480-3524. https://doi.org/10.1039/C3CS60282F
- 4. Falletta E, Rossi M, Della Pina C. The versatility of gold: From heterogeneous catalysis to biomedicine. Inorgan Chim Acta. 2022;537:120959. https://doi.org/10.1016/j.ica.2022.120959
- 5. Sankar M, Nowicka E, Richards E et al. The benzaldehyde oxidation paradox explained by the interception of peroxy radical by benzyl alcohol. Nat Commun. 2014;5(1):3332. https://doi.org/10.1038/ncomms4332
- 6. Alonso DM, Bond JQ, Dumesic JA. Catalytic conversion of biomass to biofuels. Green Chem. 2010;12(9):1493-1513. https://doi.org/10.1039/C004654J
- 7. Isahak WW, Al-Amiery A. Catalysts driving efficiency and innovation in thermal reactions: A comprehensive review. Green Technol Sustain. 2024;2(6):100078. https://doi.org/10.1016/j.grets.2024.100078
- 8. El-Moselhy MM, Ates A, Çelebi A. Synthesis and characterization of hybrid iron oxide silicates for selective removal of arsenic oxyanions from contaminated water. J Coll Interf Sci. 2017;488:335-347. https://doi.org/10.1016/j.jcis.2016.11.003
- 9. Alotaibi KM, Shiels L, Lacaze L et al. Iron supported on bioinspired green silica for water remediation. Chem Sci. 2017;8(1):567-576. https://doi.org/10.1039/c6sc02937j
- 10. Kalita A, Kashyap T, Saikia P et al. *In-situ* Iron Modified Mesoporous Silica MCM-48 for Electrochemical Energy Storage. J Por Mater. 2024;31:2067-2082. https://doi.org/10.21203/rs.3.rs-4428685/v1
- 11. Din SU, Mahmood T, Naeem A et al. A novel insight into the adsorption interactions of arsenate with a Fe–Si binary oxide. Coll J. 2019;81:469-477. https://doi.org/10.1134/S1061933X19040045
- 12. Chen X, Liang C. Transition metal silicides: fundamentals, preparation and catalytic applications. Catal Sci Technol. 2019;9(18):4785-4820. https://doi.org/10.1039/C9CY00533A

- 13. Wu X, Xianmei X, Wu Z. Oxidation of benzaldehyde to benzoic acid using heterogenous NiAl-hydrotalcite-like-compounds as the catalyst in acetic acid. Progr React Kin Mech. 2011;36(1):53-62. https://doi.org/10.3184/146867810X12910391510674
- 14. Yan H, Liu C, Luo G. Oxidation of benzaldehyde to benzoic acid. Petrol Sci Technol. 2005;23(11-12):1511-1516. https://doi.org/10.1081/LFT-200041057
- 15. Yang X, Tang S, Lu T et al. Sulfonic Acid Resin–Catalyzed Oxidation of Aldehydes to Carboxylic Acids by Hydrogen Peroxide. Synth Commun. 2013;43(7):979-985. https://doi.org/10.1080/00397911.2011.617487
- 16. Hojo J-I, Yuasa S, Yamazoe N et al. Liquid phase oxidation of benzaldehyde catalyzed by low-valent transition metal complexes. J Catal. 1975;36(1):93-98. https://doi.org/10.1016/0021-9517(75)90013-5
- 17. Zeng L. Arsenic adsorption from aqueous solutions on an Fe (III)-Si binary oxide adsorbent. Wat Qual Res J. 2004;39(3):267-275. https://doi.org/10.2166/wqrj.2004.037
- 18. Zeng L. A method for preparing silica-containing iron (III) oxide adsorbents for arsenic removal. Wat Res. 2003;37(18):4351-4358. https://doi.org/10.1016/S0043-1354(03)00402-0
- 19. Wang X, Zhang Y et al. Nanostructured semiconductor supported iron catalysts for heterogeneous photo-Fenton oxidation: a review. J Mater Chem. 2020;8(31):15513-15546. https://doi.org/10.1039/D0TA04541A
- 20. Huber DL. Synthesis, properties, and applications of iron nanoparticles. Small. 2005;1(5):482-501. https://doi.org/10.1002/smll.200500006
- 21. Lutz W, Täschner D, Kurzhals R et al. Characterization of silica gels by 29Si MAS NMR and IR spectroscopic measurements. Wiley Online Library. 2009. https://doi.org/10.1002/zaac.200900237
- 22. Ellerbrock R, Stein M, Schaller J. Comparing amorphous silica, short-range-ordered silicates and silicic acid species by FTIR. Sci Re. 2022;12(1):11708. https://doi.org/10.1038/s41598-022-15882-4
- 23. Gude K, Gun'ko VM, Blitz JP. Adsorption and photocatalytic decomposition of methylene blue on surface modified silica and silica-titania. Coll Surf A: Physicochem Eng Asp. 2008;325(1-2):17-20. https://doi.org/10.1016/j.colsurfa.2008.04.035
- 24. Zhang F, Lan J, Zhao Z et al. Removal of heavy metal ions from aqueous solution using Fe3O4–SiO2-poly (1, 2-diaminobenzene) core—shell sub-micron particles. J Coll Interf Sci. 2012;387(1):205-212. https://doi.org/10.1016/j.jcis.2012.07.066
- 25. Ward H, Cooper SS. The system benzoic acid, orthophthalic acid, water. J Phys Chem. 2002;34 (7):1484-1493. https://doi.org/10.1021/j150313a009
- 26. Schwab FW, Wichers E. Preparation of benzoic acid of high purity. J Res Nat Bur Stand. 1940;25:747-757. https://doi.org/ 10.6028/JRES.025.001

- 27. Achtler W, Dorgelo G, Fahrenfort J et al. Correlations between catalytic and thermodynamic parameters of transition metal oxides. Rec Trav Chim Pays-Bas. 1970;89(5):460-480. https://doi.org/10.1002/recl.19700890504
- 28. Wang F, Xu J, Li X et al. Liquid phase oxidation of toluene to benzaldehyde with molecular oxygen over copper-based heterogeneous catalysts. Adv Synth Catal. 2005;347(15):1987-1992. https://doi.org/10.1002/adsc.200505107
- 29. Guan X, Duan C, Wang H et al. Tuneable oxidation of styrene to benzaldehyde and benzoic acid over Co/ZSM-5. New J Chem. 2021;45(38):18192-18201. https://doi.org/10.1039/D1NJ03145G
- 30. Inoue H, Kida Y, Imoto E. Organic Catalysts. V. Specific catalytic properties of copper-iron-polyphthalocyanine in the oxidation of aldehydes. Bull Chem Soc Jap. 1968;41(3):692-696.
- 31. Yamada T, Rhode O, Takai T et al. Oxidation of aldehydes into carboxylic acids with molecular oxygen using nickel (II) complex catalyst. Chem Lett. 1991;(1):5-8. https://doi.org/10.1246/cl.1991.5
- 32. Yamazaki S. Oxidation of benzaldehydes catalyzed by methyltrioxorhenium with hydrogen peroxide. Chem Lett. 1995;24(2):127-128. https://doi.org/10.1246/cl.1995.127
- 33. Gaspar F, Nunes CD. Selective catalytic oxidation of benzyl alcohol by MoO₂ nanoparticles. Catalysts. 2020;10(2):265. https://doi.org/10.3390/catal10020265
- 34. Brink GJ, Arends IW, Sheldon RA. Green, catalytic oxidation of alcohols in water. Science. 2000;287(5458):1636-1639. https://doi.org/10.1126/science.287.5458.1636
- 35. Tandon PK, Gayatri, Sahgal S et al. Catalysis by Ir (III), Rh (III) and Pd (II) metal ions in the oxidation of organic compounds with H₂O₂. Appl Organomet Chem. 2007;21(3):135-138. https://doi.org/10.1002/aoc.1169
- 36. Zaheer A, Zahra SA, Iqbal MZ et al. Nickel-adsorbed two-dimensional Nb 2 C MXene for enhanced energy storage applications. RSC Adv. 2022;12(8):4624-4634. https://doi.org/10.1039/d2ra00014h